

Multiple Components of the Luminous Compact X-ray Source at the Edge of Holmberg II observed by *ASCA* and *ROSAT*

Takamitsu Miyaji

*Department of Physics, Carnegie Mellon University
Pittsburgh, PA 15213 (miyaji@astro.phys.cmu.edu)*

Ingo Lehmann¹

*Department of Astronomy and Astrophysics, Pennsylvania State University
University Park, PA 16802 (ilehmann@aip.de)*

and

Günther Hasinger

*Astrophysikalisches Institut Potsdam, An der Sternwarte 16
D-14482, Potsdam, Germany (ghasinger@aip.de)*

ABSTRACT

We report the results of the analysis of new *ASCA* observations and archival *ROSAT* data of the compact luminous X-ray source found at the edge of the nearby star-forming dwarf galaxy Holmberg II (UGC 4305) in the M81 group. We have found a number of new features in the X-ray properties of this source. Our new *ASCA* spectrum revealed that the X-ray emission extends to the hard band and can be best described by a power-law with a photon spectral index $\Gamma \sim 1.9$ while a $kT \sim 5$ [keV] thermal plasma with a low abundance ($\sim 0.2Z_{\odot}$) is also acceptable. The *ASCA* spectrum does not fit with a multi-color disk blackbody, unlike some off-nucleus X-ray sources with similar luminosities. The joint *ASCA-ROSAT* spectrum suggests two components to the spectrum: the hard power-law component and a warm thermal plasma ($kT \sim 0.3$ [keV]). An additional absorption over that of our galaxy is required. The wobble correction of the *ROSAT* HRI image has clearly unveiled the existence of an extended component which amounts to $27 \pm 5\%$ of the total X-ray emission.

These observations indicate that there are more than one component in the X-ray emission. The properties of the point-like component is indicative of an accretion onto an intermediate mass blackhole, unless a beaming is taking place. We argue that the extended component does not come from electron scattering and/or reflection by scattered optically-thick clouds of the central radiation. Possible explanations of this X-ray source include multiple supernova remnants feeding an intermediate-mass blackhole.

Subject headings: galaxies:dwarf — galaxies:individual (Holmberg II) — galaxies:irregular — (ISM:) supernova remnants — X-rays:galaxies

¹Also Astrophysikalisches Institut Potsdam (present address)

1. Introduction

Off-nuclear (non-AGN) point-like luminous X-ray sources, which exceed the Eddington luminosity of a usual stellar-mass compact object like neu-

tron stars and galactic binary blackholes ($L_x \gtrsim 10^{39}$ [erg s⁻¹]) in nearby galaxies have been recognized in many galaxies (Fabbiano 1989; Colbert & Mushotzky 1999; Read, Ponman & Strickland 1997). The luminosity distribution of these sources extends up to a few $\times 10^{40}$ [erg s⁻¹]. The most luminous one has been found in the nuclear region of the starburst galaxy M82 (Ptak & Griffiths 1999; Matsumoto & Tsuru 1999) reaching $\sim 10^{41}$ [erg s⁻¹]. The location of this source was recently verified to be offset from the dynamical center of the galaxy by *Chandra* (Matsumoto et al. 2001).

One interpretation of these X-ray sources is an accretion onto intermediate-mass blackholes of $10^{2-3} M_\odot$, while there are other possibilities including beaming, super-Eddington accretion, and a young supernova remnant in a dense interstellar medium. Probably they do not form a single class of X-ray sources. The spectra of many of these sources can be described by a multi-color disk blackbody model with or without additional hard tail (Makishima et al. 2000; Colbert & Mushotzky 1999). The inner disk temperatures of the sources studied by Makishima et al. (2000) are $kT \sim 1.1 - 1.8$ [keV]. Since these temperatures are higher than that from an intermediate ($10^2 M_\odot$) blackhole accretion, they proposed a picture of a spinning (Kerr) blackhole with a much smaller inner-disk radius than that of a non-spinning (Schwarzschild) one.

The luminous X-ray source in the star-forming dwarf galaxy Holmberg II (UGC 4305) is particularly peculiar among these cases in terms of the nature of the host galaxy and the location of the X-ray source. The galaxy is nearby at a distance of 3.05 Mpc, which was derived from Cepheid observations (Hoessel, Saha & Danielson 1998). It is a dwarf irregular galaxy in the M81 Group with an on-going star-formation activity. Like in other galaxies of this class, numerous HII regions are scattered throughout the galaxy (Hodge et al. 1994). The bright X-ray source, which has been cataloged in the *ROSAT* Bright Survey (RBS) (Schwope et al. 2000), is one of the most luminous X-ray source seen in dwarf galaxies ($L_x \sim 10^{40}$ [erg s⁻¹]).

It was observed three times with *ROSAT* PSPC as pointed observations and once with HRI. Zezas et al. (1999) (hereafter ZGW) studied the *ROSAT*

data on this X-ray source. Their main conclusions were: 1) The X-ray source seems point-like and located near the edge of the galaxy. Its position is consistent with one of the compact HII region complexes of the galaxy considering an uncertainty of ~ 6 arcseconds for the *ROSAT* absolute astrometry from its star tracker. A chance spatial co-incidence of this HII-region to an unrelated X-ray source of this brightness is highly unlikely ($\sim 3 \cdot 10^{-6}$). 2) The source is time variable on scales of days and years. 3) The spectrum is soft and can be fitted with a steep power-law ($\Gamma \sim 2.7$) or a thermal plasma (Raymond-Smith) of $kT \sim 0.8$ keV. Time variability suggests an accretion onto a compact object, but the luminosity is 2-4 orders of magnitude larger than typical X-ray binaries.

There is a radio-knot which is co-spatial with the HII-region in the X-ray source region. It is one of the three showing radio spectra suggestive of a non-thermal emission (Tongue & Westpfahl 1995), suggesting a recent supernova or multiple supernovae. However, currently there is no indication of a special character in the optical-radio data in this particular HII-region which is presumably associated with the compact X-ray source compared with other knots in the galaxy.

As a part of our study of a sample of apparent non-AGN galaxies which have compact luminous X-ray sources, selected from the RBS, we have made further X-ray studies of Holmberg II. In particular, we have obtained a 20 [ks] *ASCA* observation of this X-ray source in order to search for the hard X-ray signature of an AGN-like activity. In this paper, we report the results from our data analysis of our *ASCA* observation and of the *ROSAT* data from archives.

The scope of the paper is as follows. In Sect. 2, we summarize the *ASCA* and *ROSAT* observations and data used in our analysis. In Sect. 3 we report our new spectral analysis of the X-ray source by a joint *ASCA-ROSAT* PSPC analysis. In Sect. 4, we searched for an extension by applying a wobble-correction to the *ROSAT* HRI data. Long and short-term X-ray light curves are examined in Sect. 5. Finally the results are discussed in Sect. 6.

2. Observations

Holmberg II was observed with *ROSAT* five times. Firstly, it was bright in the *ROSAT* All-Sky Survey (RASS) (Voges et al. 1999) and cataloged in the RBS Schwobe et al. (2000). It was observed three times with *ROSAT* PSPC pointed observations in 1992-1993 for 3.7-11 [ks] each. Also it was observed with *ROSAT* HRI for 7.8 [ks]. The *ROSAT* pointed data have been retrieved from the High Energy Astrophysics Archival Research Center (HEASARC) located at NASA Goddard Space Flight Center.

The *ASCA* observation of Holmberg II has been made with a pointing at the X-ray source in 1999 as one of the accepted targets from our proposal in the *ASCA* EAO-6 (AO-7) program (PI=Lehmann). The brightness of the source is such that we can use the SIS FAINT mode for both the medium and high bit rates with the 1-CCD mode. Thus we chose to use the 1-CCD/FAINT modes throughout. For the subsequent analysis, we use the BRIGHT2 mode data converted from the FAINT mode. For GIS, we have used the PH mode as usual. The log of *ROSAT* and *ASCA* pointed observations is shown in Table 1.

3. X-ray Spectral Analysis using *ASCA* - *ROSAT* PSPC

3.1. Extracting *ASCA* and *ROSAT* spectra

Extraction and preparation of spectra and response matrices have been made using tools included in FTOOLS 5.0 and subsequent spectral fittings have been made using XSPEC 11.

The source spectra have been extracted from event files which have been screened using the standard screening criteria. The source-spectrum extraction radii were 6 and 3 arcminutes for the GIS and SIS respectively. The background spectra have been extracted from off-source areas from the same detector, excluding 7.5 and 3.7 arcminutes from the X-ray source for the GIS and SIS data respectively. The background subtraction have been made by scaling the background spectra by the areas of extraction, as automatically made by XSPEC. Because of the brightness of the source, the analysis is little affected by the uncertainties related to background scalings. The two GIS and two SIS spectra are co-added respec-

tively. The background spectra and response files have been generated respectively for the summed GIS 2+3 and SIS 0+1 spectra.

The *ROSAT* PSPC spectra have been extracted using an extraction radius of 1 arcminute. Background spectra have been extracted from an annular region around the source, between 1.25 and 3.75 arcminutes. One spectrum has been made for each of the three PSPC pointed observation (Table 1). We see no evidence of a spectral change among these three datasets (see below). Thus the three spectra for these three sequences have been co-added for the joint analysis with the *ASCA* data.

The *ASCA* and *ROSAT* spectra have been rebinned such that each bin contains at least 25 counts in order to utilize the χ^2 statistics during the spectral analysis. The source was bright enough for this re-binning process without sacrificing the resolution.

3.2. Spectral Analysis

The channel energy ranges used for the analysis are 0.15-2 keV, 0.6-10 keV, and 1.0-7 keV for the *ROSAT* PSPC, *ASCA* GIS, and *ASCA* SIS, respectively. Because of the calibration uncertainties related to the radiation damage, we have ignored *ASCA* SIS channels below 1 keV.

Firstly, we have verified the basic fitting results of ZGW with joint fits to the three PSPC spectra, where all model parameters are joined except for the global normalization. As observed by ZGW, slight variations of the global normalization have been observed. This is discussed in Sect. 5. When all parameters are separately fit for the three datasets, the best fit parameters are always consistent with the joint ones within errors. This warrants that we can use the summed spectra for *PSPC* for further analysis.

Next we have made a spectral analysis of *ASCA* only (GIS & SIS). We have tried to fit the spectra with three models: (A1) a single power-law, (A2) a thermal plasma using the XSPEC *mekal* model, and (A3) a disk blackbody (Mitsuda et al. 1984) (XSPEC model *diskbb*), where “A” stands for *ASCA*. The best-fit parameters are shown in Table 2 and fit residuals are shown in Fig. 1. The single power-law of photon index $\Gamma \sim 1.9$ gave the best fit without inclusion of any absorption. The photon indices for separate fits to the gave

$\Gamma = 1.85 \pm 0.07$ and 1.87 ± 0.07 for GIS and SIS, respectively (N_{H} fixed to 0). The agreement verifies the goodness of our background subtraction. The 90% upper-limit to the column density of the absorbing gas was $N_{\text{H}} \leq 1.3 \cdot 10^{21} \text{ [cm}^{-2}\text{]}$. The thermal plasma model with $kT \sim 5 \text{ [keV]}$ also gave a good fit with $\chi^2/\nu = 0.84$. We have obtained a heavy element abundance of $Z = 0.2 \pm 0.2 Z_{\odot}$, which is marginally consistent with the O/H ratio of ~ 0.4 (relative to solar) for this galaxy (Hunter & Gallagher 1985). However note that the metallicity of the source of X-ray emission does not necessarily be equal to that of some average for the HII regions scattered throughout the galaxy and that the hard X-ray mainly measures the iron abundance, which does not necessarily match with that of oxygen.

The multicolor disk blackbody model failed to fit the *ASCA* data as shown in Fig. 1(c). Thus the disk-blackbody component does not dominate the hard X-ray emission observed by our *ASCA* observation, unlike the cases of, e.g., IC 342 source 1 and NGC 1313 source B studied by Makishima et al. (2000). The power-law index of the *ASCA* spectrum is much harder than that of *ROSAT* PSPC spectrum ($\Gamma \approx 2.7$; ZGW), which has response in $E \lesssim 2 \text{ keV}$.

Finally, we have made a joint spectral analysis using all the *ROSAT* PSPC and *ASCA* GIS/SIS data. We have summed all the three PSPC spectra for the joint spectral fits. We have joined all the model parameters except for the global normalization as before. Because the *ROSAT* spectrum, covering a lower energy range, is much softer than that of *ASCA*, we have tried models with hard power-law ($\Gamma \sim 1.9$) with some soft excess and an absorbing column. Adding a softer power-law component did not give a satisfactory fit. As the soft component, we have tried the thermal plasma and disk blackbody models. As shown in Table 2, both ‘‘Power-law+Thermal’’ (J1) and ‘‘Power-law+Disk blackbody’’ (J2) models gave reasonable fits. Note that the abundance of the thermal plasma have been fixed to 0.4 (see above) for J1. When this was a free parameter, the fit could not constrain it. In both J1 and J2, the absorbing column was $N_{\text{H}} \sim 0.7 - 1 \cdot 10^{21} \text{ [cm}^{-2}\text{]}$, which exceeds the galactic value implied by the 21cm data of $N_{\text{H}} \sim 3 \cdot 10^{20}$ (Dicky & Lockman 1990), indicating an absorbing component within Holmberg

II. The soft excess component, which can either be described as a $kT \sim 0.3 \text{ [keV]}$ thermal plasma or a $kT_{\text{in}} \sim 0.2 \text{ [keV]}$ disk blackbody spectrum, has 20-30% of the total 0.5-2 keV total luminosity. The *ROSAT* and *ASCA* spectra are shown with folded models and residuals in Fig. 2 for J1. The total luminosity of the X-ray source is $\approx 1.0 \cdot 10^{40} \text{ [erg s}^{-1}\text{]}$ in the 0.1-10 keV after correcting for absorption (GIS normalization). This corresponds to an Eddington luminosity of $\sim 80[M_{\odot}]$.

For the fit J2, the GIS normalization of the disk blackbody component gives $r_{\text{in}}\sqrt{\cos\theta} = 3500 - 7500 \text{ [km]}$, where r_{in} is the inner disk radius, θ is the viewing angle and the 90% confidence error was searched for by allowing all other variable parameters to vary. Assuming $r_{\text{in}} = 3 R_{\text{S}}$, where R_{S} is the Schwarzschild radius, this corresponds to a blackhole mass of $10\text{-}25 (\cos\theta)^{-0.5}[M_{\odot}]$, while Colbert & Mushotzky (1999) pointed out that the r_{in} estimation based on the disk blackbody within XSPEC is likely to be underestimated. Further discussion is made in Sect. 6

We have also tried a two-thermal plasma model fit (J3), where the relative abundances of two thermal plasma have been fixed to equal. This model gave an acceptable fit but with a hard thermal component (Thermal_h) with $kT_{\text{h}} \sim 6 \text{ [keV]}$ and a soft thermal component (Thermal_s) with $kT_{\text{s}} \sim 0.3 \text{ [keV]}$. In this case, the fitted abundance was very low $Z = 0.02^{+0.03}_{-0.01}$. We did not find a satisfactory fit for the model where the hard component is a thermal plasma and the soft component is a power-law.

One caveat on our joint fitting analysis is a possible cross-calibration problem. Iwasawa, Fabian & Nandra (1999) found that the *ROSAT* PSPC spectrum is much softer than that of *ASCA* SIS for the simultaneous observations of NGC 5548 ($\Gamma = 2.35$ for *ROSAT* PSPC versus $\Gamma = 1.95$ for *ASCA* SIS). This might have been partially caused by the soft excess combined with the spectral resolution of PSPC or there may be real cross-calibration problems. The origin of this discrepancy is inconclusive. In our case, the difference of $\Delta\Gamma \sim 0.7$ between the *ROSAT* PSPC and *ASCA* GIS spectra is much larger than that Iwasawa, Fabian & Nandra (1999) observed for a similar *ASCA* index. Thus there certainly is a soft component over the extrapolation of the hard power-law even in case the discrepancy observed

by Iwasawa, Fabian & Nandra (1999) was solely caused by calibration problems.

4. *ROSAT* HRI Wobble-Correction and Spatial Extension

There are wobble-phase dependent systematic errors with the aspect solution for the *ROSAT*, which could lead to a detection of spurious extended component in the HRI data (Harris et al. 1998; Morse 1994). This has lead to ZGW make a conservative conclusion that they had detected no extension in the HRI image. We have applied a correction for this effect by creating images in 10 wobble-phases, centering each of these images independently, and re-constructing the image using the centering information Lehmann et al. (1999). The original and corrected HRI images are shown in Fig. 3. The faint knot seen in the NW in the original HRI image has disappeared in the corrected image. This reconstruction worked very well down to an HRI count rate of ~ 0.1 [cts s $^{-1}$] for a large number of stars, but can be even used for fainter sources (Crawford et al. 1999).

The radial profile of the wobble-corrected HRI image has been compared with the theoretical HRI PSF from David et al (1995) and the re-calibrated HRI PSF in Fig. 4. The re-calibrated HRI PSF was derived from wobble-corrected HRI images of 21 stars from the RBS Schwobe et al. (2000). The re-calibrate HRI PSF shows a slightly deviation from the theoretical PSF in the radial range between 10 and 30 arcseconds. The comparison of the radial profile with both PSF's indicates an extended component. Subtracting the re-calibrated PSF, $27 \pm 5\%$ (1σ error) of the X-ray emission is in the extended component and most of the excess comes from a radius of $\sim 10''$, corresponding to ~ 150 [pc].

5. Variability

The *ASCA* GIS flux in the 0.5-2 keV band calculated using the spectral model J1 have been compared with the previous *ROSAT* observations. Because *ASCA* GIS is sensitive only above 0.6 keV, while *ROSAT* HRI has no spectral resolution and sensitive in 0.2-2 keV, we have made separate long-term light curves for the 0.2-2 and 0.5-2 keV bands. These are shown in Fig. 5. The fluxes from *ROSAT* are slightly different from Fig. 3. of ZGW

probably because of the difference in spectral models. As seen in Fig. 5, there is a 30% decrease in flux between the first (April 1992) and third (March 1993) PSPC pointed observations and a factor of ~ 2 increase towards the HRI observation (Oct, 1994). The source brightness came back to a flux close to the PSPC observation during the *ASCA* observation in 1999. This does not necessarily mean that the source is variable at a time scale of “years”, rather it means that there is a variability at a timescale longer than the elapsed time of a single observation ($10^5 - 10^6$ [s]).

We also searched for evidence of time variability in the *ASCA* data. First, we have defined the combined Good Time Intervals (GTI), which consist of the intersection of GTI's from all the SIS and GIS detectors. We have used channels corresponding to 0.6-10 keV for the GIS's and 0.7-7 keV for the SIS's respectively. For each detector, binned source and background light curves have been extracted using a 1024 second binsize. The extraction regions are the same as those of the spectral analysis. For each time bin, only the interval overlapped with the combined GTI have been used to calculate the countrate. The background-subtracted light curves have been co-added to make the final light curve. There is no significant correlation between the background-subtracted source light curve and the background light curve. This also warrants goodness of the background subtraction.

The resulting light curve is shown with the best χ^2 -fit constant value in Fig. 6. No point is more than 2σ away from the constant value and $\chi^2/\nu = 22.2/26$. Thus there is no evidence for variability at time scales between 10^3 and 10^4 seconds in the *ASCA* data. Separate light curves for the hard ($E \geq 2$ [keV]) and soft ($E < 2$ [keV]) bands did not show any sign of variability either. This is in contrast to the *ROSAT* light curves reported by ZGW, which show a convincing case of gradual decrease of flux by a factor of ~ 3 over 2×10^5 seconds during the second pointed PSPC observation and less convincing indications of shorter timescale variabilities.

6. Discussion

Our analysis suggests at least two-components of the X-ray emission. An extended and a point-

like component have been revealed by the spatial analysis. The variability also provides evidence for at least a compact component. The joint *ASCA/ROSAT* spectral analysis suggests a non-thermal power-law component plus a warm thermal component or a moderately low temperature disk blackbody component. The overall spectrum can also be described as a superposition of two thermal components with a very low metallicity. However, the variability observed in this object argues against total thermal origin of the X-ray source.

The X-ray source at the edge of Holmberg II shows unusual characters, even given the large number of off-nuclear X-ray sources in nearby galaxies at similar luminosities. While most of the X-ray sources studied by Colbert & Mushotzky (1999) reside in the nuclear region, this is at the very edge of a dwarf galaxy. Unlike a number of off-nuclear sources studied by Makishima et al. (2000), hard X-ray emission is not dominated by a disk blackbody component with $kT_{\text{in}} \gtrsim 1$ [keV]. If the soft excess component comes from a disk blackbody emission, the implied blackhole mass from the normalization of this component is $10\text{-}25 (\cos \theta)^{-0.5} [M_{\odot}]$ assuming a Schwarzschild blackhole (see Sect. 3). However, estimating the mass from the temperature $kT_{\text{in}} \sim 0.2$ [keV] using Eq. (12) of Makishima et al. (2000), we obtain $\sim 10^4 [M_{\odot}]$. This large discrepancy argues against the disk-blackbody interpretation of the soft excess, even though we consider the underestimation of the mass pointed out by Colbert & Mushotzky (1999), nearly edge on viewing angle, and spinning of the blackhole.

One of the most surprising results from our analysis is that these two (or more) bright X-ray components co-exist in a compact region in one of the numerous HII regions and no other X-ray source with a comparable brightness exists in other part of the galaxy. All other X-ray sources scattered throughout the galaxy, which are either supernova remnants or X-ray binaries, have luminosities of $L_x \lesssim 10^{37}$ [erg s⁻¹ cm⁻²] (Kerp & Walter 2000). Thus it is unlikely that the two (or more) components have independent origins. The possible explanations of this X-ray source with observed multiple components are:

(a) A supernova remnant (SNR) or a composite

of SNRs (the $kT \sim 0.3$ [keV] extended thermal component) feeds an intermediate mass blackhole with gas.

- (b) An accretion onto a stellar-mass compact object, e.g., similar to galactic blackhole X-ray binaries, beaming towards our line of sight, is embedded in an SNR or a composite of SNRs.
- (c) The non-thermal power-law and the soft excess components (possibly blackbody emission from the accretion disk around an intermediate-mass blackhole) come from the same compact region while the extended component is caused by scattering/reflection of the central source.

The flat radio spectrum (Tongue & Westpfahl 1995) in the region of this X-ray source shows an existence of a supernova remnant or a composite of supernova remnants. This supports the possibilities (a) or (b). However, the extended component is too luminous for thermal emission from a single (or a few) supernova remnant(s) (SNR), considering its size of ~ 200 pc and its 0.5-2 keV luminosity of a few $\times 10^{39}$ [erg s⁻¹]. A single SNR can only be at this luminosity when it is very young ($\lesssim 10^2$ years) (Schlegel 1994; Schlegel et al. 1999) and thus it cannot have grown into this scale size nor can feed the intermediate-mass blackhole located 200 [pc] away. Thus more than a few supernova remnants are needed to make the extended structure, which also feeds the blackhole causing the variable, non-thermal emission. From our current data, we are not able to distinguish whether the central source represents an accretion onto an intermediate-mass blackhole or a stellar mass compact object (e.g. X-ray binaries) with beaming towards our line of sight.

The possibility (c) is not likely for the following reasons. The possibility that electron-scattering by surrounding diffuse gas is the origin of the extended emission has the following difficulty. Scattering gas with a column density of $N_{\text{H}} \gtrsim 10^{23} - 10^{24}$ [cm⁻²] is required to account for the $\sim 30\%$ extended component. The gas would cause heavy photoelectric absorption unless the scattering diffuse gas is highly ionized (Wilson et al. 1992; Elvis et al. 1990). If the gas was thermally ionized, the temperature of the gas

must be greater than a few million degrees [K] in order that the absorption features due to a column density of $N_{\text{H}} = 10^{23}$ [cm $^{-2}$] is not visible in the *ASCA* spectrum. For demonstration, we assume a uniform sphere of gas of 200 [pc] in radius filled with hot ionized gas with a column density of $N_{\text{H}} = 10^{23}$ [cm $^{-2}$] from the central source. Such a sphere of thermal gas would produce X-ray emission which is several orders of magnitude larger than observed. Photoionization also cannot be a valid explanation, because the lower limit of the ionization parameter required to be consistent with the *ASCA* spectrum also requires several orders of magnitude larger luminosity for the ionizing source. We also consider a picture where the surfaces of optically-thick molecular clouds scattered throughout the region (giant molecular clouds where star forming activities are embedded) reflect the radiation from the central source, while our line of sight to the central source is not blocked by any of them. This picture also has a similar difficulty. In order to attain sufficient reflectivity in the *ROSAT* band ($E \lesssim 2$) [keV], the surface of the clouds have to be highly ionized. Using the XSPEC model “pexriv” (Magdziarz & Zdziarski 1995), we estimate that an ionization parameter of $\xi \equiv L/(nR^2) >$ a few hundred [erg cm s $^{-1}$] is required to have the reflectivity of more than 20-30% in this band. For a central ionizing source luminosity of $L \sim$ a few $\times 10^{40}$ [erg s $^{-1}$], at a distance of $R = 200$ [pc], this ionization parameter corresponds to a gas density at the surfaces of the clouds of $n \lesssim 10^{-3}$ [cm $^{-3}$]. This is much lower than that of a usual interstellar medium and scattered clouds of this density cannot be optically thick.

If the intermediate-mass blackhole picture of this X-ray source is the case, there is a question of its formation. Taniguchi et al. (2000) discussed possible origins of the off-nucleus “intermediate-mass” blackholes presumably responsible for off-nuclear luminous X-ray sources and their preferred model was multiple mergings of stellar remnants (stellar-mass blackholes and neutron stars). Matsushita et al. (2000) found a molecular superbubble in the vicinity of a similar off-nuclear X-ray source in M82, suggesting that an intensive star formation is connected to the formation of an intermediate-mass blackhole. This may be the case for the compact component of the X-ray

source discussed here because of the intense star-forming activity in the region. However, the question remains as to why there is only one such X-ray source in this galaxy and not at the locations of other numerous HII regions. Probably the X-ray emission is a short-lived phenomenon, where an intermediate mass blackhole (similar things may exist in many star-forming regions) is fed by the passing of a shell of dense gas induced by multiple supernova explosions.

Chandra (scheduled as a GT target by Murray) and XMM-Newton (GT target by Watson) observations of this source will certainly improve our knowledge of this peculiar X-ray source. The Chandra observation can make spatially resolved X-ray spectroscopy and reveal whether the non-thermal component corresponds to the point-source and thermal to the extended component or it has a more complicated structure. The XMM-Newton observation would give a better spectral information with a much better statistics and much less cross-calibration uncertainties in the $E \lesssim 1$ keV region, where multiple components are apparent. It will also give variability information at short timescales.

7. Conclusions

We summarize the main conclusions of our analysis:

1. New *ASCA* and archival *ROSAT* data of the X-ray source in Holmberg II have been analyzed.
2. The combined *ASCA* and *ROSAT* spectrum shows can be described as a $\Gamma \sim 2$ power-law and a soft excess which can either be described as a $kT \sim 0.3$ [keV] thermal plasma or $kT_{\text{in}} \sim 0.2$ disk blackbody. We argue against the disk blackbody interpretation of the soft excess component based on the inconsistency between the luminosity and the temperature.
3. The wobble-corrected *ROSAT* HRI image indicates $\sim 25\%$ of the X-ray emission is extended at a scale of $\gtrsim 10''$ ($\sim 25\%$). Variability in the *ROSAT* data shows that the point-like component probably comes from accretion onto a compact object.

4. It is remarkable that this multiple-component X-ray source is the only one with a similar strength among the numerous HII regions in the galaxy with a similar nature. It is natural to suppose that these two components are related.
5. Possible explanations of the nature of the X-ray source include multiple supernova remnants (extended component) feeding the accretion onto an intermediate-mass blackhole. We cannot, however, exclude the possibility that the central source is a beamed radiation from an accretion onto a stellar mass (usual X-ray binaries) object. We argue against a picture where electron scattering or reflection by scattered optically-thick clouds of the central source makes the extended X-ray emission.

This research have made use of data and software obtained from the High Energy Astrophysics Archival Research Center (HEASARC) located at NASA Goddard Space Flight Center. The authors appreciate the effort of *ASCA* and *ROSAT* teams for having created and operated these superb observatories. The authors thank the referee, Hironori Matsumoto for his careful review and useful comments.

REFERENCES

- Anders E. & Grevesse N. 1989, *Geochimica et Cosmochimica Acta* 53, 197
- Colbert, E. J. M. & Mushotzky, R. F. 1999, *ApJ*, 519, 89
- Crawford, C. S., Lehmann, I., Fabian, A. C., Bremer, M. N., & Hasinger, G. 1999, *MNRAS*, 308, 1159
- David, L.P., Harnden, F.R., Kearns, K.E., & Zombek, M.V. *The ROSAT High Resolution Imager (HRI)* (Cambridge:SAO)
- Dickey, Lockman 1990, *ARA&A* 28, 215
- Elvis, M., Fasnacht, C., Wilson, A. S. & Briel, U. 1990, *ApJ*, 361, 459
- Fabbiano, G. *ARA&A*, 28, 215

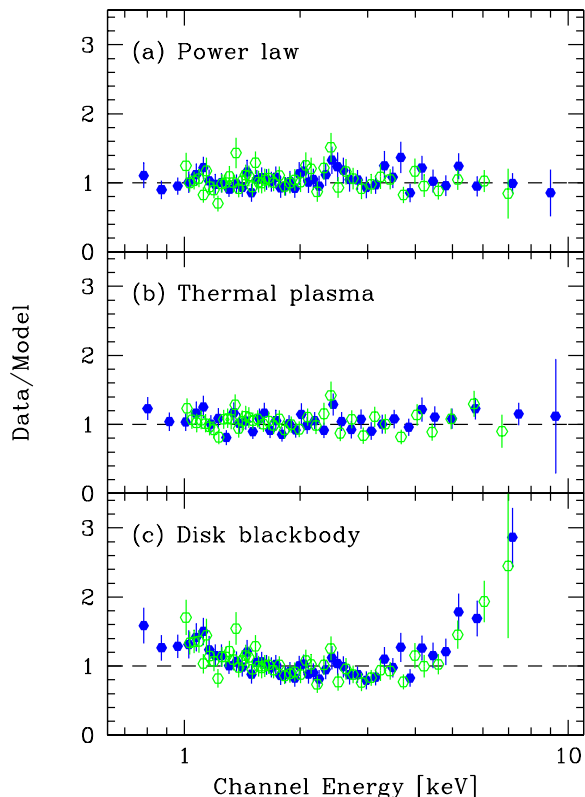


Fig. 1.— The residuals for three model fits of the *ASCA* GIS (filled circles)/SIS (open circles) spectra are shown in terms of the ratio of the data and model. The models are (a) a single power-law, (b) a thermal plasma, (c) a disk blackbody. See Table 2 for the best-fit parameters.

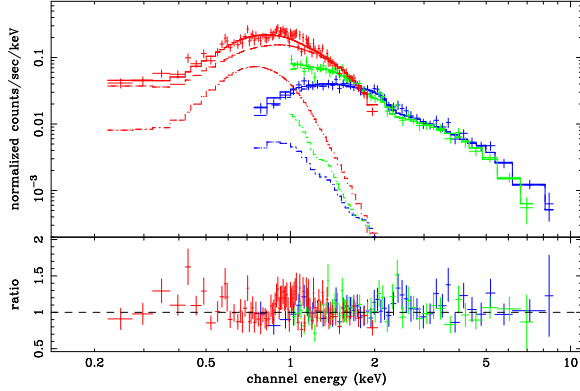


Fig. 2.— The *ASCA* GIS (0.6-10 keV)/SIS (1-7 keV) and *ROSAT* PSC (0.2-2 keV) spectra are shown with folded model predictions for the best-fit power-law plus thermal (MEKAL) model with absorption (Fit J1). The fit residuals are shown in the lower panel in terms of the ratio of the data and the model. The error bars show 1σ errors. The detector corresponding to each spectrum can be identified by the energy range. The power-law (dashed) and thermal (dot-dashed) components of the folded model have also been shown separately for each instrument.

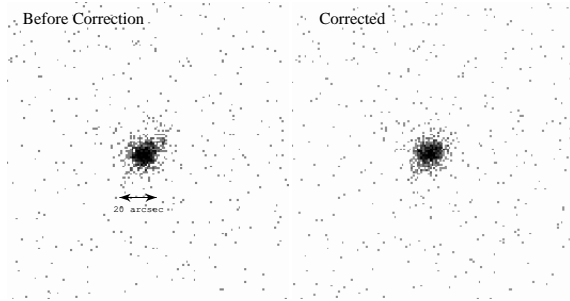


Fig. 3.— The *ROSAT* HRI image of Holmberg II before (north is up, east is left) and after the wobble aspect correction. Note that a faint knot seen at the north-west in the original image have disappeared after the correction.

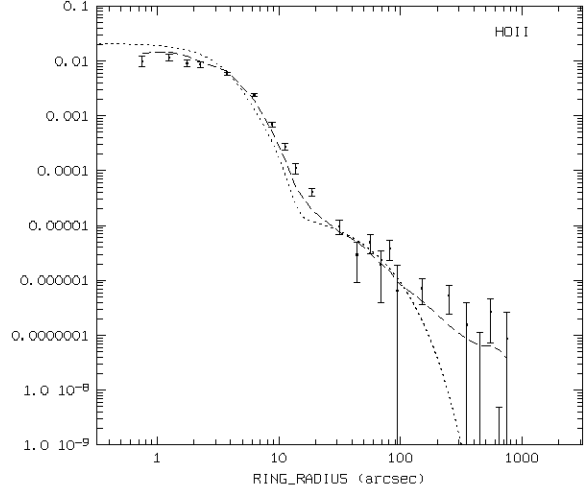


Fig. 4.— The wobble-corrected radial profile of the compact X-ray source in Holmberg II is compared with the theoretical HRI PSF (dotted line) and the re-calibrated HRI PSF (dashed line). The bars mark 1σ errors of the data points. An extended component is clearly seen in $\gtrsim 10$ arcseconds.

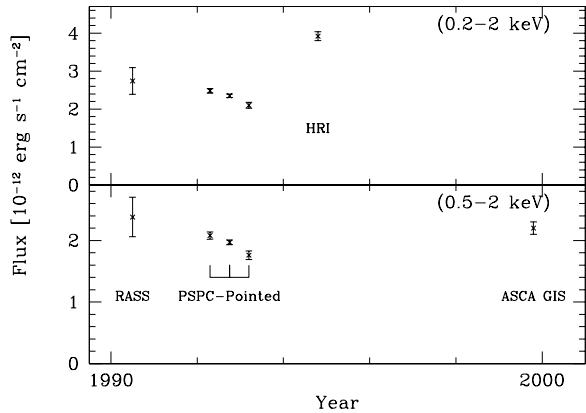


Fig. 5.— The long-term light curves of Holmberg II from 1990-1999 in the 0.2-2 keV (*ROSAT* PSC and HRI) and 0.5-2 keV (*ROSAT* PSC and *ASCA* GIS) bands. The error bars are 1σ .

- Harris, D. E., Silverman, J. D., Hasinger, G. & Lehmann, I. 1998, *A&AS*, 133, 431
- Hodge P., Strobel N.V., Kennicutt R.C. 1994, *PASP*, 106, 309
- Hoessel, J. G., Saha, A. & Danielson, G. E. 1998, *AJ*, 115, 573
- Hunter, D. A. & Gallagher, J. S. 1985, *ApJS*, 58, 533
- Iwasawa, K., Fabian, A. C. & Nandra, K. 1999, *MNRAS*, 307, 611
- Kerp J. & Walter F. et al. 2000 in “X-ray astronomy 2000”, eds. R. Giacconi, L. Stella, S. Serio, *ASP Conf. Series*, in press (astro-ph/0012255)
- Lehmann I., et al. 1999 in “Highlights in X-ray Astronomy”, MPE report 272, (Garching:MPE), 209
- Magdziarz, P. & Zdziarski, A. A. 1995, *MNRAS*, 273, 837
- Makishima, K. et al. 2000, *ApJ*, 535, 632
- Matsumoto, H. & Tsuru, T. G. 1999, *PASJ*, 51, 321
- Matsumoto, H. et al. 2001, *ApJL* 547, L25
- Matsushita, S., Kawabe, R., Matsumoto, H., Tsuru, T. G., Kohno, K., Morita, K., Okumura, S. K. & Vila-Vilaró, B. 2000, *ApJ*, 545, L107
- Mitsuda, K. et al. 1984, *PASJ*, 36, 741
- Morrison, R. & McCammon, D. 1983, *ApJ*, 270, 119
- Morse, J. A. 1994, *PASP*, 106, 675
- Ptak A. & Griffiths R.E 1999, *ApJ*, 517, L85
- Puche D., Westpfahl D.J, Brinks E. 1992, *AJ*, 103, 1841
- Read, A. M., Ponman, T. J. & Strickland, D. K. 1997, *MNRAS*, 286, 626
- Schlegel, E. M. 1994, *ApJ*, 424, L99
- Schlegel E. M. et al. 1999, *AJ* 118, 2689
- Schwope A. D., Hasinger G., Lehmann I. et al. 2000, *Astron. Nachr.*, 321, 1
- Taniguchi, Y., Shioya, Y., Tsuru, T. G. & Ikeuchi, S. 2000, *PASJ*, 52, 533
- Tongue, T. D. & Westpfahl, D. J. 1995, *AJ*, 109, 2462
- Voges, W., et al. 1999, *A&A*, 349, 389
- Wilson, A. S., Elvis, M., Lawrence, A. & Bland-Hawthorn, J. 1992, *ApJ*, 391, L75
- Zezas A.L., Georgantopoulos I., Ward M.J. 1999, *MNRAS*, 308, 302 (ZGW)

TABLE 1
LOG OF *ROSAT* AND *ASCA* OBSERVATIONS

Detector(Mode)	Sequence	Start Date	Exposure [ks]
<i>ROSAT</i> PSPC	rp600140n00	14-APR-1992	7.3
“ “	rp600431n00	29-OCT-1992	11.6
“ “	rp600431a00	14-MAR-1993	3.7
<i>ROSAT</i> HRI	rh600745n00	17-OCT-1994	7.8
<i>ASCA</i> GIS(PH)	ad77075000	21-OCT-1999	16.5
<i>ASCA</i> SIS (ICCD/FAINT)	“	“	16.5(S0)/16.3(S1)

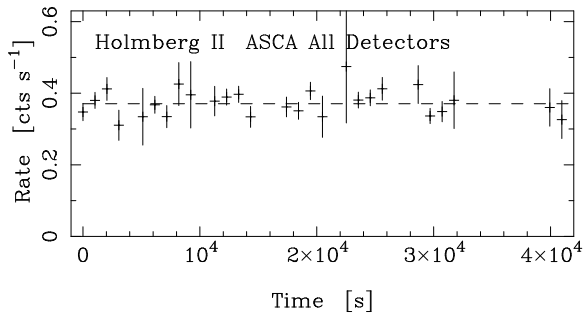


Fig. 6.— The *ASCA* light curve of Holmberg II with 1σ errors. Background-subtracted source counts for the all four detectors have been co-added. The energy ranges are 0.6-10 and 0.7-7 keV for the GIS and SIS respectively. The dashed line shows the best-fit constant value.

TABLE 2
RESULTS OF THE SPECTRAL ANALYSIS

Model	Parameters
<i>ASCA</i> GIS & SIS Data	
PL (A1)	$K_G = 1.0*$; $K_S = .87 \pm .05$; $\Gamma = 1.87 \pm 0.05$; $F_{p12} = 2.5 \pm 0.1$; $\chi^2/\nu = \mathbf{0.83}$ (170./206)
Thermal (A2)	$K_G = 1.0*$; $K_S = .86 \pm .05$; $kT = 4.8 \pm 0.4$; $F_{t12} = 2.2 \pm .1$; $Z = 0.2 \pm 0.2$; $\chi^2/\nu = \mathbf{0.84}$ (208./206)
Disk BB (A3)	$K_G = 1.0*$; $K_S = .87 \pm .05$; $kT_{in} = 1.19 \pm 0.05$; $F_{d12} = 1.9 \pm .1$; $\chi^2/\nu = \mathbf{1.34}$ (276./206);
<i>ROSAT</i> PSPC & <i>ASCA</i> GIS/SIS	
(PL+Thermal) · Abs. (J1)	$K_G = 1.0*$; $K_S = .87 \pm .05$; $K_P = .79 \pm .06$; $\Gamma = 1.91 \pm .04$; $F_{p12} = 2.6 \pm .2$; $kT = .30 \pm .05$; $Z = 0.4*$; $F_{t12} = .67 \pm .17$; $N_{H20} = 7.9 \pm .06$; $\chi^2/\nu = \mathbf{1.02}$ (324./317)
(PL+Disk BB) · Abs. (J2)	$K_G = 1.0*$; $K_S = .86 \pm .04$; $K_P = .78 \pm .04$; $\Gamma = 1.88 \pm .07$; $F_{p12} = 2.6 \pm .2$; $kT_{in} = .17 \pm .02$; $F_{d12} = 1.0 \pm .2$ $N_{H20} = 9.6 \pm 1.1$; $\chi^2/\nu = \mathbf{1.04}$ (329./317)
(Thermal_h+Thermal_s) · Abs. (J3)	$K_G = 1.0*$; $K_S = .87 \pm .05$; $K_P = .79 \pm .04$; $kT_h = 5.9^{+1.4}_{-.9}$; $F_{th12} = 2.0 \pm .1$; $kT_s = .35 \pm .05$; $F_{ts12} = 1.4 \pm .2$; $Z = .02^{+.03}_{-.01}$; $N_{H20} = 8.5 \pm 1.0$; $\chi^2/\nu = \mathbf{1.00}$ (317./317)

NOTE.— Free parameters of fit are shown with 90% errors ($\Delta\chi^2 = 2.7$). Fixed parameter values are followed by an asterisk (*). K : Overall normalization factor for each detector/observation. Detectors are identified with a subscript (G:GIS S:SIS P:PSPC). The normalization is expressed as a 0.5-2 keV flux (unabsorbed) in units of $[10^{-12}\text{erg s}^{-1}\text{cm}^{-2}]$. Model Components— **PL**: Power-law with a photon index of Γ and a 0.5-2 keV flux of F_{p12} . **Thermal**: Thermal plasma using the XSPEC *mekal* model with a plasma temperature kT [keV], a metal abundance Z in solar units, where the solar abundance is from Anders & Grevesse (1989), and a 0.5-2 keV flux of F_{t12} . For Model J3, the two thermal components are notified by subscripts h (hard) and s (soft) respectively. **Disk BB**: The multicolor disk (Mitsuda et al. 1984) (the XSPEC model *diskbb*) with an innerdisk temperature kT_{in} and 0.5-2 keV flux of F_{m12} . **Abs**: Absorption by neutral gas using the XSPEC model *wabs* (Morrison & McCammon 1983) with hydrogen column density N_{H20} [10^{20}cm^{-2}].